

Ground-state properties of a triangular triple quantum dot connected to superconducting leads

Akira Oguri,¹ Izumi Sato,¹ Masashi Shimamoto,¹ and Yoichi Tanaka²

¹ Department of Physics, Osaka City University, Osaka 558-8585, Japan

² Condensed Matter Theory Laboratory, RIKEN, Saitama 351-0198, Japan

Abstract. We study ground-state properties of a triangular triple quantum dot connected to two superconducting (SC) leads. In this system orbital motion along the triangular configuration causes various types of quantum phases, such as a Kondo effect with a four-fold degenerate state and the Nagaoka ferromagnetic mechanism, depending on the electron filling. The ground state also evolves as the Cooper pairs penetrate from the SC leads. We describe the phase diagram in a wide range of the parameter space, varying the gate voltage, the couplings between the dots and leads, and also the Josephson phase between the SC gaps. The results are obtained in the limit of large SC gap, carrying out exact diagonalization of an effective Hamiltonian. We also discuss a classification of the quantum states according to the fixed point of the Wilson numerical renormalization group (NRG). Furthermore, we show that the Bogoliubov zero-energy excitation determines the ground state of a π Josephson junction at small electron fillings.

1. Introduction

Triangular triple quantum dot (TTQD) is one of the multi-dot systems that has intensively been studied in these years. One of the interesting features of this system is rich internal degrees of freedom that emerge through orbital motion along the triangular configuration and also from several different possible concentrations of occupying electrons. Furthermore, the number of the conducting channels and the way the leads are connected to the TTQD also give a variety to ground state and low-energy excitations. For these reasons, various kinds of Kondo effects and quantum phase transition have been predicted for this system [1–8].

This report focuses on the interplay and competition between the electron correlation and superconductivity [9–13]. Specifically, we consider the TTQD that is embedded in a Josephson junction between two superconducting (SC) leads as illustrated in Fig. 1 [14, 15]. We explore the wide parameter space of this junction to clarify how the Cooper pairs penetrating into the TTQD realize various quantum phases in the presence of a large Coulomb interaction.

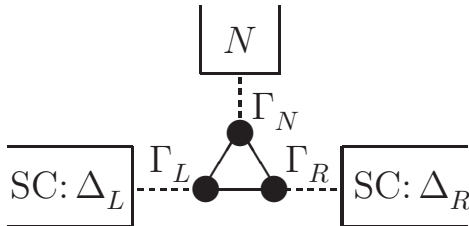


Figure 1. Triangular triple quantum dots (●) coupled to one normal (N) and two superconducting leads (L, R) with the gaps $\Delta_{L/R} = |\Delta_{L/R}| e^{i\theta_{L/R}}$. Here, $\Gamma_\nu \equiv \pi\rho v_\nu^2$ with ρ the density of states of the leads $\nu = L, R, N$, and v_ν the tunneling matrix element.

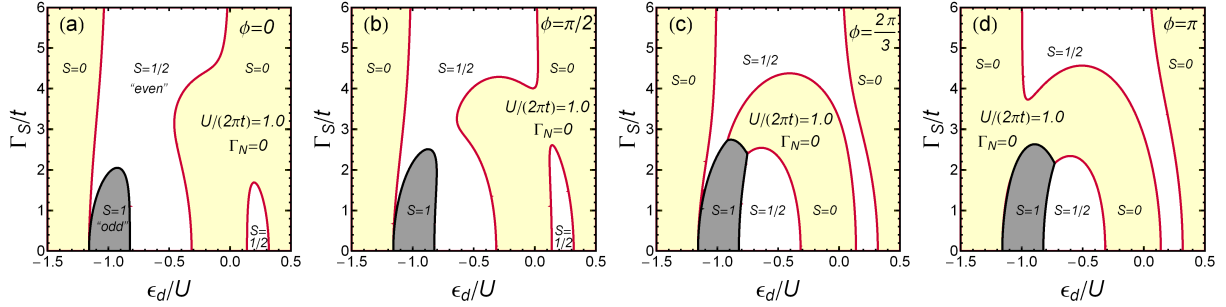


Figure 2. Ground-state phase diagram of the TTQD for $\Gamma_N = 0$, is plotted in an ϵ_d vs Γ_S plane for (a) $\phi = 0$, (b) $\phi = \pi/2$, (c) $\phi = 2\pi/3$, and (d) $\phi = \pi$, for relatively large Coulomb interaction $U = 2\pi t$. The eigenstates can be classified according to the total spin S , which takes values of $S = 0, 1/2$, and 1 in the yellow, white, and gray regions, respectively.

2. Model & Formulation

We start with the Hamiltonian, given in the form $H = H_{\text{QD}} + H_{\text{T}} + H_{\text{lead}}$ with

$$H_{\text{QD}} = -t \sum_{\langle ij \rangle} \sum_{\sigma} \left(d_{i\sigma}^{\dagger} d_{j\sigma} + d_{j\sigma}^{\dagger} d_{i\sigma} \right) + \sum_i \sum_{\sigma} \epsilon_d n_{d,i\sigma} + U \sum_i n_{d,i\uparrow} n_{d,i\downarrow}, \quad (1)$$

$$H_{\text{T}} = \sum_{\nu=N,L,R} \sum_{\sigma} v_{\nu} \left(\psi_{\nu\sigma}^{\dagger} d_{\nu\sigma} + d_{\nu\sigma}^{\dagger} \psi_{\nu\sigma} \right), \quad \psi_{\nu\sigma} \equiv \int_{-D}^D d\varepsilon \sqrt{\rho} c_{\varepsilon\alpha m} \quad (2)$$

$$H_{\text{lead}} = \sum_{\nu=N,L,R} \sum_{\sigma} \int_{-D}^D d\varepsilon \varepsilon c_{\varepsilon\nu\sigma}^{\dagger} c_{\varepsilon\nu\sigma} + \sum_{\alpha=L,R} \int_{-D}^D d\varepsilon \left(\Delta_{\alpha} c_{\varepsilon\alpha\uparrow}^{\dagger} c_{\varepsilon\alpha\downarrow}^{\dagger} + \text{H.c.} \right). \quad (3)$$

where $d_{i\sigma}^{\dagger}$ is the creation operator an electron with energy ϵ_d and spin σ in the quantum dot at site i , U is the Coulomb interaction U and $n_{d,i\sigma} \equiv d_{i\sigma}^{\dagger} d_{i\sigma}$. Similarly, $c_{\varepsilon\nu\sigma}^{\dagger}$ creates an electron in the lead $\nu = L, R, N$, and is normalized as $\{c_{\varepsilon\nu\sigma}, c_{\varepsilon'\nu'\sigma'}^{\dagger}\} = \delta_{\nu\nu'} \delta_{\sigma\sigma'} \delta(\varepsilon - \varepsilon')$. We assign the same label for the dot, $i = L, R, N$, as the one for the adjacent lead that is coupled via the tunneling matrix element v_{ν} with $\rho = 1/(2D)$ and $\Gamma_{\nu} \equiv \pi \rho v_{\nu}^2$. The superconducting gap $\Delta_{\alpha} = |\Delta_{\alpha}| e^{i\theta_{\alpha}}$ induces the Josephson current between the two SC leads for finite phase differences $\phi \equiv \theta_R - \theta_L$.

Since this Hamiltonian has a number parameters to be explored, we consider the case where $\Gamma_L = \Gamma_R (\equiv \Gamma_S)$ and $|\Delta_L| = |\Delta_R| (\equiv \Delta_{\text{SC}})$. Specifically, we concentrate on the case where the SC gap is much larger than the other energy scales $\Delta_{\text{SC}} \gg \max(\Gamma_S, \Gamma_N, U, |\epsilon_d|)$ but D , and the quasi-particle excitations in the continuum energy region above the SC gap are projected out. Nevertheless, the essential physics of the SC proximity is still preserved, and in the limit of $\Delta_{\text{SC}} \rightarrow \infty$ it is described by an effective Hamiltonian

$$H_{\text{eff}} = H_{\text{QD}} + \sum_{\alpha=L,R} \left(\Delta_{d,\alpha} d_{\alpha\uparrow}^{\dagger} d_{\alpha\downarrow}^{\dagger} + \Delta_{d,\alpha}^* d_{\alpha\downarrow} d_{\alpha\uparrow} \right), \quad \Delta_{d,\alpha} \equiv \Gamma_S e^{i\theta_{\alpha}}. \quad (4)$$

The static SC pair potential $\Delta_{d,\alpha}$ is induced in the TTQD, the amplitude of which is determined by the coupling strength $|\Delta_{d,\alpha}| \equiv \Gamma_S$ while the phase θ_{α} preserves that of the SC hosts [?, ?]. In the present report, we concentrate on the $\Gamma_N = 0$ case where the normal lead is disconnected.

3. Ground states & Fixed points for the TTQD connected to two SC leads

In this section, we describe how the ground state of the TTQD coupled to two SC leads evolves as the Hamiltonian parameters ϵ_d and Γ_S vary. Figure 2 shows the phase diagram for the ground

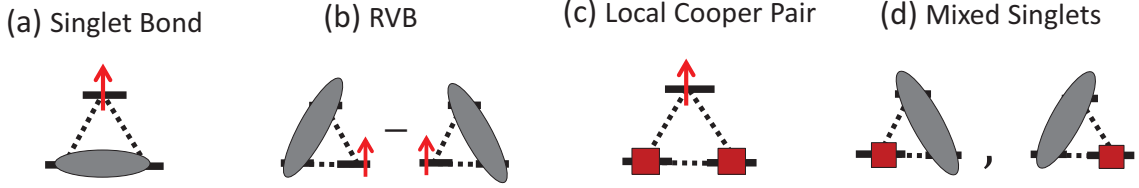


Figure 3. Schematic pictures of the fixed-point wavefunctions near half-filling, defined in Eqs. (5)–(9) for $\Gamma_N = 0$. The gray oval denotes the singlet bond, and the brown square denotes the local Cooper pair (LCP). The mixed singlets (d) have two independent configurations.

state of H_{eff} for relatively large interaction $U = 2\pi t$. In the horizontal direction the average number of electrons N_{tot} in the TTQD increases as ϵ_d decreases, while in the vertical direction the SC proximity becomes large as Γ_S increases. Specifically, for $\Gamma_S = 0$, the occupation discontinuously changes near $\epsilon_d/U \simeq -1.2, -0.8, -0.3, 0.1$, and 0.3 . Correspondingly, level crossing occurs between the states of different total spins, $S = 1/2$ and $S = 0$, or $S = 1$ Nagaoka state that is caused by orbital motions along the triangular configuration [2, 6, 7]. We see that the ground state evolves sensitively to the phase difference ϕ for intermediate values of the SC proximity, around $\Gamma_S/t \simeq 3.0$, near half-filling $\epsilon/U \simeq -0.5$ where $N_{\text{tot}} \simeq 3.0$. This reflects properties of the wavefunctions, which are schematically illustrated in Fig. 3 and can be expressed in the form

$$|\Phi_{SB}\rangle = d_{N\uparrow}^\dagger \left(d_{L\uparrow}^\dagger d_{R\downarrow}^\dagger - d_{L\downarrow}^\dagger d_{R\uparrow}^\dagger \right) |0\rangle, \quad (5)$$

$$\begin{aligned} |\Phi_{RVB}\rangle &= \frac{1}{\sqrt{6}} \left\{ d_{R\uparrow}^\dagger \left(d_{N\uparrow}^\dagger d_{L\downarrow}^\dagger - d_{N\downarrow}^\dagger d_{L\uparrow}^\dagger \right) - d_{L\uparrow}^\dagger \left(d_{N\uparrow}^\dagger d_{R\downarrow}^\dagger - d_{N\downarrow}^\dagger d_{R\uparrow}^\dagger \right) \right\} |0\rangle \\ &= \frac{1}{\sqrt{6}} \left(d_{N\uparrow}^\dagger d_{L\downarrow}^\dagger d_{R\uparrow}^\dagger + d_{N\uparrow}^\dagger d_{L\uparrow}^\dagger d_{R\downarrow}^\dagger - 2d_{N\downarrow}^\dagger d_{L\uparrow}^\dagger d_{R\uparrow}^\dagger \right) |0\rangle, \end{aligned} \quad (6)$$

$$|\Phi_{LCP}\rangle = d_{N\uparrow}^\dagger \left(e^{-i\frac{\theta_L}{2}} - e^{i\frac{\theta_L}{2}} d_{L\uparrow}^\dagger d_{L\downarrow}^\dagger \right) \left(e^{-i\frac{\theta_R}{2}} - e^{i\frac{\theta_R}{2}} d_{R\uparrow}^\dagger d_{R\downarrow}^\dagger \right) |0\rangle, \quad (7)$$

$$|\Phi_{\text{mix},1}\rangle = \frac{1}{2} \left(e^{-i\frac{\theta_L}{2}} - e^{i\frac{\theta_L}{2}} d_{L\uparrow}^\dagger d_{L\downarrow}^\dagger \right) \left(d_{N\uparrow}^\dagger d_{R\downarrow}^\dagger - d_{N\downarrow}^\dagger d_{R\uparrow}^\dagger \right) |0\rangle, \quad (8)$$

$$|\Phi_{\text{mix},2}\rangle = \frac{1}{2} \left(e^{-i\frac{\theta_R}{2}} - e^{i\frac{\theta_R}{2}} d_{R\uparrow}^\dagger d_{R\downarrow}^\dagger \right) \left(d_{N\uparrow}^\dagger d_{L\downarrow}^\dagger - d_{N\downarrow}^\dagger d_{L\uparrow}^\dagger \right) |0\rangle. \quad (9)$$

These states also represent typical fixed points of the Wilson numerical renormalization group (NRG) near half-filling. Specifically, the two spinful states, $|\Phi_{SB}\rangle$ and $|\Phi_{RVB}\rangle$, constitute a four-fold degenerate ground state for $\Gamma_S = 0$ in the strong interaction case $U \gg t$ [1–8]. Note that the SB and RVB can be categorized into the even and odd parity states, respectively, with respect to a vertical axis passing through the apex site of the triangle (see Fig. 1).

Infinitesimal SC proximity lifts this degeneracy of the singlet bond (SB) and the resonating valence bond (RVB) states as seen in Fig. 4 which shows Γ_S dependence of the eigenvalues near half-filling $\epsilon_d = -0.5U$ for $U = 2\pi t$. Detailed features of the eigenvectors can be deduced from the overlap integrals with the fixed-point wavefunctions defined in Eqs. (5)–(9):

$$|\langle \Phi_{SB} | \Psi_{1\text{st}}^{S=1/2} \rangle|^2, \quad |\langle \Phi_{RVB} | \Psi_{1\text{st}}^{S=1/2} \rangle|^2, \quad |\langle \Phi_{LCP} | \Psi_{1\text{st}}^{S=1/2} \rangle|^2, \quad \sum_{j=1}^2 |\langle \Phi_{\text{mix},j} | \Psi_{1\text{st}}^{S=0} \rangle|^2. \quad (10)$$

Here, $|\Psi_{1\text{st}}^{S=0}\rangle$ and $|\Psi_{1\text{st}}^{S=1/2}\rangle$ are the lowest eigenstates in the $S = 0$ and $1/2$ subspaces, respectively. Some typical examples are shown in Fig. 5. For small proximities $\Gamma_S/t \lesssim 2.0$,

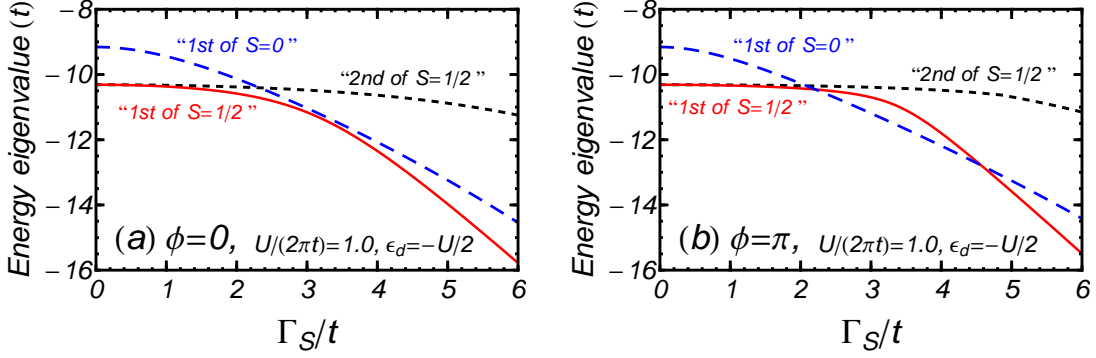


Figure 4. Eigenvalues of H_{eff} vs Γ_S , for (a) $\phi = 0$ and (b) $\phi = \pi$, at $\epsilon_d = -U/2$ and $U = 2\pi t$. First two energies are shown for the subspace of spin $S = 1/2$, while only the lowest one is shown for $S = 0$.

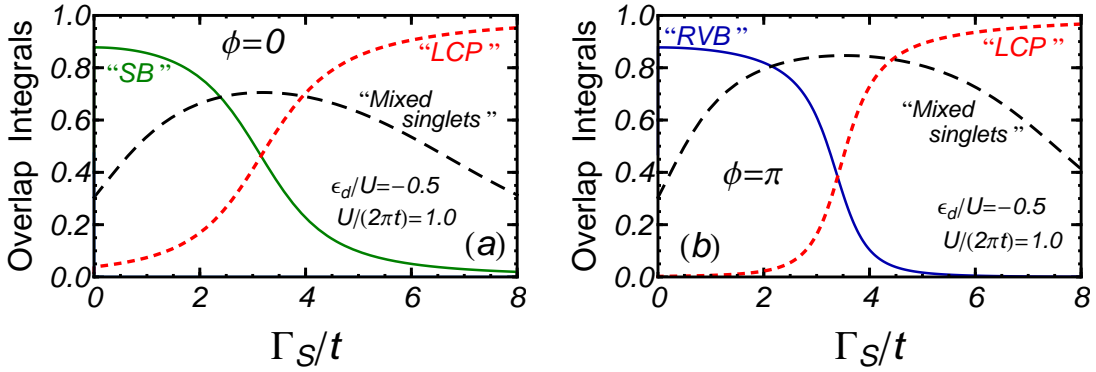


Figure 5. Overlap integrals, $|\langle \Phi_{SB} | \Psi_{1\text{st}}^{S=1/2} \rangle|^2$, $|\langle \Phi_{RVB} | \Psi_{1\text{st}}^{S=1/2} \rangle|^2$, $|\langle \Phi_{LCP} | \Psi_{1\text{st}}^{S=1/2} \rangle|^2$, and $\sum_{j=1}^2 |\langle \Phi_{\text{mix},j} | \Psi_{1\text{st}}^{S=0} \rangle|^2$, are plotted vs Γ_S for (a) $\phi = 0$ and (b) $\phi = \pi$. $|\Psi_{1\text{st}}^{S=0}\rangle$ and $|\Psi_{1\text{st}}^{S=1/2}\rangle$ are the lowest-energy states in the $S = 0$ and $1/2$ subspaces, respectively.

the singlet-bond state $|\Phi_{SB}\rangle$ dominates the ground state for $\phi = 0$, whereas the RVB dominates for $\phi = \pi$. Therefore, in this region the ground state must evolve from the SB to the RVB as ϕ increases, as it will be discussed later.

The overlap integrals $|\langle \Phi_{SB} | \Psi_{1\text{st}}^{S=1/2} \rangle|^2$ and $|\langle \Phi_{RVB} | \Psi_{1\text{st}}^{S=1/2} \rangle|^2$ decrease as Γ_S/t increases, and a crossover occurs for both $\phi = 0$ and π . Then, for large proximities $\Gamma_S/t \gtrsim 4.0$, the local Cooper pairing $|\Phi_{LCP}\rangle$, in which the SC proximities at the bottom and the local spin at the apex of the triangle coexist, determines the ground-state properties. We can also see in the intermediate region near $\Gamma_S/t \simeq 3.0$ that the lowest singlet eigenstate $|\Psi_{1\text{st}}^{S=0}\rangle$ has a large overlap with the mixed singlet states $|\Phi_{\text{mix},j}\rangle$, in which the local Cooper pair at the bottom and a singlet bond in the oblique side share the dots in the triangular configuration. This type of the singlet becomes the ground state in the center of the phase diagrams in Figs. 2 (a)–(d), and it explains why the $S = 0$ region expands as ϕ increases for intermediate Γ_S near half-filling. This is also consistent with the behavior of the eigenvalues seen in Fig. 4 (b), in which $|\Psi_{1\text{st}}^{S=0}\rangle$ becomes the ground state around $\Gamma_S/t \simeq 3.0$ for $\phi = \pi$.

For small Γ_S near half-filling, the ground state must change from the SB to the RVB at finite ϕ , as mentioned. We see in Fig. 6 (a) that this occurs near $\phi \simeq 2\pi/3$ for $U = 2\pi t$. As ϵ_d increases, the fixed-point state showing the greatest overlap changes from the SB to the RVB near $\epsilon_d/U \simeq -0.6$. Therefore, the magnetic $S = 1/2$ ground state can be classified according to

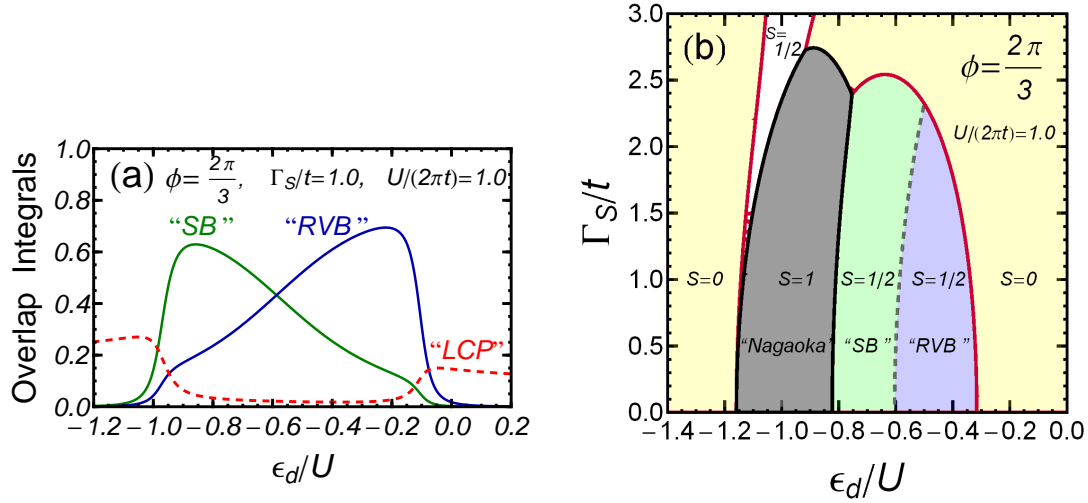


Figure 6. Grand states for $\phi = 2\pi/3$ and $U = 2\pi t$. (a): ϵ_d dependence of overlap integrals at $\Gamma_S/t = 1.0$. (b): Enlarged phase diagram, in which the dashed line traces the points where the overlap integral for the SB and that for RVB coincide, as $|\langle \Phi_{SB} | \Psi_{1st}^{S=1/2} \rangle|^2 = |\langle \Phi_{RVB} | \Psi_{1st}^{S=1/2} \rangle|^2$.

these overlap integrals. Figure 6 (b) shows an enlarged phase diagram for $\phi = 2\pi/3$. The dashed line represents the boundary, on which $|\langle \Phi_{SB} | \Psi_{1st}^{S=1/2} \rangle|^2 = |\langle \Phi_{RVB} | \Psi_{1st}^{S=1/2} \rangle|^2$. This boundary line penetrates into the $S = 1/2$ region from the adjacent $S = 0$ region on the right, and will move towards the $S = 1$ Nagaoka region on the left as ϕ increases further.

4. Bogoliubov zero-energy excitation

Another characteristics of the ground-state phase diagrams, shown in Fig. 2 for $U = 2\pi t$, is that the boundary between the $S = 0$ and $S = 1/2$ regions at $\epsilon_d/U \simeq 0.3$ is connected for large ϕ ($\gtrsim 0.56\pi$), while the two regions are separated for small ϕ ($\lesssim 0.55\pi$). Note that this change takes place for small electron fillings: the quantum dots are almost empty on the right side of this phase boundary, and the first electron enters into the TTQD as ϵ_d passes through the boundary. Therefore, around this boundary the Coulomb interaction U can be treated perturbatively, and thus the Bogoliubov quasiparticles $\gamma_{k\sigma}$ which diagonalize the noninteracting Hamiltonian play an essential role,

$$H_{\text{eff}} \xrightarrow{U=0} \sum_{k=1}^3 \sum_{\sigma} E_k \gamma_{k\sigma}^{\dagger} \gamma_{k\sigma} + \text{const.} \quad (11)$$

Figure 7 (a) shows the three energy levels of E_k for $\phi = 0$ (dashed line) and $\phi = \pi$ (solid line). We see that the lowest excitation energy becomes zero for $\phi = \pi$ at $\epsilon_d/t \simeq 1.88$ and $\Gamma_S = t$. The zero mode, where $E_k = 0$, emerges in the parameter space for $\phi = \pi$ along the line,

$$\Gamma_S^2 \epsilon_d + (\epsilon_d - 2t)(\epsilon_d + t)^2 = 0. \quad (12)$$

On this line, which is also shown in Fig. 7 (b), the excitation has a four-fold degeneracy that can be classified according to the occupation number of the zero mode. The Coulomb interaction U lifts this degeneracy, and then a singly occupied $S = 1/2$ doublet becomes ground state in the region around the line of the zero-energy excitations. This explains the characteristics of the phase diagrams, Fig. 2 (c) and (d), near $\phi = \pi$: the boundary between the $S = 0$ and $S = 1/2$ regions near $\epsilon_d/U \simeq 0.3$ does not enclose itself but stretches out towards the direction of positive large Γ_S 's.

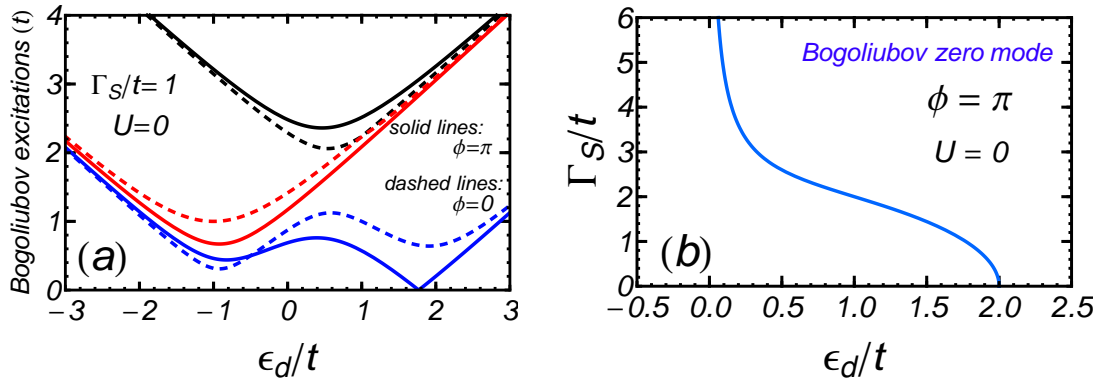


Figure 7. (a): Bogoliubov excitations E_k vs ϵ_d for $U = 0$ and $\Gamma_S/t = 1.0$: the solid and dashed lines represent the energy levels for $\phi = \pi$ and $\phi = 0$, respectively. (b): Zero-energy mode of $E_k = 0$ emerges at $\phi = \pi$ along the blue line in the ϵ_d vs Γ_s plane.

5. Summary

We have studied in detail the ground states of the TTQD embedded in a Josephson junction between two SC leads. Specifically, various quantum phases emerging in a wide parameter space have been classified according to the fixed points which include new ones, the LCP and the mixed singlets, describing the SC proximities. The results of the overlap integrals clarify the correspondence between the ground state and the fixed points, and give a clear physical interpretation to the phase diagram. Effects of the normal lead on low-energy properties will be discussed elsewhere.

Acknowledgments

We would like to thank Yasuhiro Yamada and Rui Sakano for discussions. This work is supported by the JSPS Grant-in-Aid for Scientific Research (C) (No. 26400319) and (S) (No. 26220711). Numerical computation was partly carried out at Yukawa Institute Computer Facility.

References

- [1] T. Kuzmenko, K. Kikoin and Y. Avishai, Phys. Rev. Lett. **96**, 046601 (2006).
- [2] A. Oguri, Y. Nisikawa, Y. Tanaka, and T. Numata, J. Magn. & Magn. Mater. **310**, 1139 (2007).
- [3] R. Žitko and J. Bonča, Phys. Rev. B **77**, 245112 (2008).
- [4] A. K. Mitchell, T. F. Jarrold, and D. E. Logan, Phys. Rev. B **79**, 085124 (2009).
- [5] E. Vernek, C. A. Büsser, G. B. Martins, E. V. Anda, N. Sandler and S. E. Ulloa, Phys. Rev. B **80**, 035119 (2009).
- [6] T. Numata, Y. Nisikawa, A. Oguri, and A. C. Hewson, Phys. Rev. B **80**, 155330 (2009).
- [7] A. Oguri, S. Amaha, Y. Nishikawa, T. Numata, M. Shimamoto, A. C. Hewson and S. Tarucha, Phys. Rev. B **81**, 075404 (2011).
- [8] M. Koga, M. Matsumoto, and H. Kusunose, J. Phys. Soc. Jpn. **82**, 093706 (2013).
- [9] A. Martín-Rodero and A. Levy Yeyati, Adv. Phys. **60**, 899 (2011).
- [10] J. Bauer, A. Oguri, and A. C. Hewson, J. Phys.: Condes. Mat. **19**, 486211 (2007).
- [11] Yoichi Tanaka, N. Kawakami, and A. Oguri, J. Phys. Soc. Jpn. **76**, 074701 (2007); **77**, 098001(E) (2008).
- [12] R. S. Deacon, Yoichi Tanaka, A. Oiwa, R. Sakano, K. Yoshida, K. Shibata, K. Hirakawa, and S. Tarucha, Phys. Rev. B **81**, 121308 (2010).
- [13] R. Maurand and C. Schönenberger, Physics **6**, 75 (2013).
- [14] M. Governale, M. G. Pala, and J. König, Phys. Rev. B **77**, 134513 (2008).
- [15] A. Oguri, Yoichi Tanaka, and J. Bauer, Phys. Rev. B **87**, 075432 (2013).